JOURNAL OF GEOPHYSICAL RESEARCH, VOL. 99, NO. C1, PAGES 825–841, JANUARY 15, 1994

# Numerical simulation of vorticity waves in the nearshore

A. Falqués and V. Iranzo

Departament de Física Aplicada, Universitat Politècnica de Catalunya, Barcelona, Spain

**Abstract.** A numerical method based on spectral expansions is given for the computation of vorticity waves arising from shear instability of a longshore current. This method allows for any mean flow profile and any beach topography (remaining constant alongshore and with a straight shoreline). The shallow-water equations are considered without any assumption about the sea surface (such as rigid lid), and dissipative terms accounting for bottom friction and/or eddy viscosity are included. A numerical simulation for some flow profiles that are quite realistic in the surf zone and for several bathymetries is presented. For inviscid flow the predictions of the Bowen and Holman (1989) analytical model for a very simplified geometry are found to give rise to the main features. However, the details in the flow and depth profiles are found to significantly influence the instability curves, especially for a barred beach. For the fastest growing mode, the wavelength is between 1.7 and 2.7 times the width of the mean current $l$. Frequencies of about $0.09f_s$, where $f_s$ is the maximum shear at the sea face of the current profile, and an $e$-folding time of the exponential growth that is roughly equal to the wave period are obtained. The phase speed is between 0.5 and 0.7 of the mean current peak. Dissipation has a considerable effect on the wavenumber span and the growth rate of the instability, so reasonably constant values of the eddy viscosity and realistic values of the Chezy coefficient can entirely remove the instability. The phase speed of neutral shear waves is analytically found to be equal to the mean flow velocity at the cross-shore location where the potential vorticity has an extremum. This velocity is found to give an estimate of the phase speed of growing modes. We found that the rigid-lid assumption tends to overestimate the growth rates by an amount which depends on the maximum Froude number of the mean flow. The instability curves and the dispersion lines for a free surface converge towards the rigid-lid ones when the Froude number decreases, and the rigid-lid assumption is therefore valid for a low Froude number.

## 1. Introduction

Waves at subincident frequencies in the nearshore have long been considered to be solely gravity waves, either leaky modes or trapped edge modes. Recently, a new class of alongshore progressive waves, named shear or vorticity waves, has been recognized, with the potential vorticity of the mean longshore flow instead of gravity as the restoring force. These waves therefore appear only in the presence of strong longshore flows [*Oltman-Shay et al.*, 1989; *Howd et al.*, 1991*a*, *b*]. Their periods and alongshore wavenumbers are of the order of $10^2$ s and $10^2$ m, respectively, and for a given frequency $f$ their wavelength $\lambda$ is substantially shorter than the gravity wave wavelength, that is, $\lambda < g\beta/2\pi f^2$, where $\beta$ is the beach slope, and $g$ is gravitational acceleration. These waves are very coherent and energetic, dominating the $f < 0.01$ Hz frequency band or far-infragravity band. While the amplitude of the surface oscillations is small, $O$(1 cm), the horizontal velocity amplitudes can be greater than 30 cm/s. These waves have little dispersion, and they propagate downstream with a phase speed of about half the mean current peak. As suggested by *Bowen and Holman* [1989] (hereinafter referred to as BH), vorticity waves may play an important role in cross-shore mixing and mean longshore current dissipation. In addition, a more extensive analysis by *Putrevu and Svendsen* [1992] indicates that this mixing is mainly located shoreward of the breaker line.

BH proposed a simple model for vorticity waves as resulting from shear instability of a steady mean longshore current. Their approach considers a plane horizontal bottom, and under the assumption of a rigid-lid (nondivergence), the linear inviscid shallow-water equations are transformed into the Rayleigh equation of the classical shear instability theory. Then, assuming a mean flow with piecewise linear shear, a growing (or unstable) mode can be obtained analytically. This analytical solution matches the properties of the observed vorticity waves fairly well. A natural frequency scaling by $f_s$, the maximum shear at the sea face of the longshore current, is found, with a representative frequency given by $f \sim 0.07f_s$. Wavelengths are of the order of $2l$, where $l$ is the width of the longshore current, and a phase speed roughly equal to $V_{max}/3$ is found. Similar results were obtained by *Dodd and Thornton* [1990] for a somewhat less simplified geometry with a piecewise planar bathymetry.

These analytical models give rise to the main features of the instability because the basic structure of the actual potential vorticity profile is preserved. However, the influence of considering realistic flow and depth profiles instead of idealized ones and the influence of dissipation or removing the rigid-lid assumption may have some importance. Solving



Paper number 93JC02214.
0148-0227/94/93JC-02214$05.00

the governing equations to account for the effects of realistic conditions requires numerical procedures. To this end, *Putrevu and Svendsen* [1992] solved the governing equations numerically with a rigid-lid and for inviscid flow, allowing for any smooth current profile and for any bathymetry. Their numerical technique cuts off the semi-infinite domain of the cross-shore coordinate (imposing the far offshore boundary condition at a finite distance instead of at infinity) and considers a finite-difference scheme to transform the governing equation into an algebraic linear eigenproblem. A considerable sensitivity to variations in the bottom topography unnoticed by the previous analytical models was found. This sensitivity is especially striking for barred beaches. Moreover, larger growth rates of the instability for barred beaches than for monotone ones were in general obtained. As opposed to the analytical results for simplified geometries, more than one instability mode was found, and the instability curves were found to have an (0, 0) intercept, so they did not have a minimum positive unstable wavenumber. Phase speeds of about 0.5 to 0.6 times the mean current peak were obtained.

A similar numerical work was carried out by *Dodd et al.* [1992] using mean flow and bathymetry from two real beaches, a barred one at Duck, North Carolina (SUPERDUCK experiment), and a plane one at Santa Barbara, California (Nearshore Sediment Transport Studies (NSTS)). Dodd et al. included bottom friction in their model equations. Its effect was found to be important, resulting in a decrease in the span of unstable wavenumbers and in growth rates. Their paper provides a comparison between numerical simulation and field data, which were found to be in good quantitative agreement at SUPERDUCK. Results from NSTS were less conclusive. In line with *Putrevu and Svendsen* [1992], Dodd et al.'s results suggest that shear instabilities may be a more common feature on barred beaches than on plane ones.

Like the articles by *Putrevu and Svendsen* [1992] and *Dodd et al.* [1992], the present paper is aimed at providing an analysis of shear instability with more realistic conditions by means of numerical simulation. A smooth mean current profile is also considered, as are a number of depth profiles including nonplanar topography. Frequency against wavenumber and growth rate against wavenumber curves are given. The spatial structure of the waves, including flow pattern, surface elevation, and phase shifts between fluid variables, is investigated. As opposed to the previous approaches, the rigid-lid assumption is removed and the effects of dissipation are included by means of a simple model with a constant eddy viscosity. A term accounting for bottom friction through a Chezy coefficient is also included in the governing equations (this bottom friction modeling is implicitly based on the strong-current assumption, as opposed to the weak-current assumption used by Dodd et al.). In addition, our numerical method is quite different from the previous methods. This is very interesting, because the coincidence between the results from different numerical models allows us to reach a higher level of numerical evidence for these results. We essentially follow a technique similar to that used for edge wave calculation in the presence of longshore current [*Falqués and Iranzo*, 1992] but with some improvements. The shallow-water equations are transformed into a linear algebraic eigenproblem by means of spectral expansions. Owing to longshore periodicity, discretization in this direction is achieved by trigonometric functions (in fact, because of linearity, longshore wavenumbers are decoupled, and only one Fourier mode is needed in each expansion). Cross-shore, a domain decomposition technique is used, cutting the whole [0, ∞) interval into two parts: a finite one and a semi-infinite one. Then Chebyshev polynomials are used in the former, and rational Chebyshev functions are used in the latter. This technique makes it possible to obtain a maximum resolution where the maximum strength of the instability is located and gives rise to greater efficiency than the similar rational Chebyshev collocation method previously used in edge wave computation. The present numerical technique has also been found to be more efficient than the finite-difference schemes previously used. Near the transition, because the governing equations become singular, this method loses its accuracy for almost neutral waves (and this is so also for the approaches of *Putrevu and Svendsen* [1992] and *Dodd et al.* [1992]. In this case we use an overshooting technique but take into account the singularity at the cross-shore location where the mean flow velocity equals the phase speed of the wave. In addition to this numerical work, an analytical estimate of the phase velocity is given by using some asymptotic analysis and an energy identity obtained in previous work [*Falqués and Iranzo*, 1992]. Moreover, the classical energy analysis of the Drazin and Howard semicircle theorem [*Drazin and Reid*, 1981] is extended to allow for a free upper surface.

## 2. Formulation

Cartesian axes are chosen with the mean free surface as the $(x - y)$ plane, with $x$ pointing offshore, $y$ being directed along a straight shoreline, and $z$ pointing upward. Consider the shallow-water equations for momentum and mass conservation [*van Rijn*, 1987]:

$$u_t + uu_x + vu_y = -g\eta_x + \tau_x/\rho + \varepsilon(u_{xx} + u_{yy}) \tag{1a}$$

$$v_t + uv_x + vv_y = -g\eta_y + \tau_y/\rho + \varepsilon(v_{xx} + v_{yy}) \tag{1b}$$

$$s_t + (su)_x + (sv)_y = 0 \tag{1c}$$

where $u$ and $v$ are the horizontal depth-averaged velocities, and $\rho$ and $g$ stand for water density and gravity acceleration, respectively. The free surface and the bottom are given by $z = \eta(x, y, t)$ and $z = h(x, y)$; hence $s = \eta - h$ stands for the height of the water column. The external forces are assumed to be

$$\tau_x = \tau_{sx} - \frac{\rho g}{sC^2} u(u^2 + v^2)^{1/2}$$

$$\tau_y = \tau_{sy} - \frac{\rho g}{sC^2} v(u^2 + v^2)^{1/2} \tag{2}$$

allowing for bottom friction by means of the Chezy coefficient $C$, where $\tau_s$ are the driving forces balancing dissipation due to wind stresses or radiation stresses from wave breaking. Finally, $\varepsilon$ stands for a constant viscosity coefficient. Let us now assume a beach given by $z = -H(x)$ with $H(0) = 0$ and $H(x) > 0$ $x > 0$ and a basic steady flow given by $u = 0$, $v = V(x)$ with an undisturbed free surface $\eta = 0$. When we consider dissipation, this steady flow is possible if there

is an external net longshore force given by $\tau_y = -\rho\varepsilon V_{xx}$ and no cross-shore net stresses $\tau_x = 0$.

Assume now a small perturbation of the basic flow with the form of a longshore progressive wave:

$$u = u'(x)\ \exp\ [ik(y - ct)]$$

$$v = V(x) + v'(x)\ \exp\ [ik(y - ct)]$$

$$\eta = \eta'(x)\ \exp\ [ik(y - ct)]$$

where $c = c_r + ic_i$, and $\lambda = 2\pi/k$ is the wavelength. The phase speed is given by $c_r$, the frequency is given by $\omega_r = 2\pi f = c_r k$, and the growth rate is given by $\omega_i = c_i k$.

Then, taking into account (2) and upon linearization with respect to the perturbation, from (1) we obtain

$$ik(V - c)u' + \frac{g}{HC^2} Vu' + \varepsilon(k^2 - \partial_x^2)u' + g\eta_x' = 0 \qquad (3a)$$

$$V_x u' + ik(V - c)v' + 2\frac{g}{HC^2} Vv' + \varepsilon(k^2 - \partial_x^2)v' + ikg\eta' = 0 \qquad (3b)$$

$$(Hu')_x + ikHv' + ik(V - c)\eta' = 0 \qquad (3c)$$

Henceforth, for simplicity we drop the prime on the perturbations $u'$, $v'$, and $\eta'$. If we assume inviscid flow, that is, $\varepsilon = 0$ and $g/C^2 = 0$, we have from (3)

$$u = i\frac{g}{k(V - c)}\eta_x \qquad v = -\frac{g}{(V - c)}\eta - \frac{gV_x}{k^2(V - c)^2}\eta_x \qquad (4)$$

Then, by dropping $u$ and $v$, a single governing equation follows:

$$\left(\frac{gH}{(V - c)^2}\eta_x\right)_x + \left(1 - \frac{gH}{(V - c)^2}\right)k^2\eta = 0 \qquad (5)$$

$$x \in [0, \infty)$$

Equation (5) was obtained in a previous paper [*Falqués and Iranzo*, 1992], but it was handled only for neutral waves, $c_i = 0$.

In all the previous works, the rigid-lid assumption, that is, $\eta_t$ is negligible with respect to horizontal fluxes, was considered. Under this hypothesis, (1$c$) allows us to use a stream function.

$$Hu = -\psi_y \qquad Hv = \psi_x$$

Then, assuming inviscid flow, one can also find a single governing equation from (3$a$) and (3$b$):

$$(V - c)\left(\psi_{xx} - k^2\psi - \frac{H_x\psi_x}{H}\right) - \left(\frac{V_x}{H}\right)_x H\psi = 0 \qquad (6)$$

In the case of a plane horizontal bottom, $H_x = 0$, this equation reduces to the Rayleigh equation of the classical shear flow instability theory [*Drazin and Reid*, 1981].

Let us now see what boundary conditions must be applied to system (3). For inviscid flow, these equations can be converted into the single equation (5). The origin, $x = 0$, is a singular point of this equation, and, as appeared in edge wave calculation [*Iranzo and Falqués*, 1992], the proper equation may be considered a boundary condition at this point, giving correct results. Therefore we have imposed the proper equations (3) at $x = 0$ as boundary conditions for inviscid flow. Taking into account the Chezy terms does not modify the order of the equations, and the same boundary conditions have thus been considered. In dealing with eddy viscosity, the boundary conditions to be applied at the shoreline are not clear. Since $u$ and $v$ are depth-averaged velocities, owing to the mobility of the shoreline the no-slip condition, which may be applied at the sea bottom for three-dimensional modeling, is not obvious. After some trials we chose the equations without the viscosity terms as boundary conditions at $x = 0$. This choice led to a numerically well-posed problem insofar as it gave stable results for an increasing number of discretization nodes. At infinity, $u(\infty) = v(\infty) = \eta(\infty) = 0$ have been taken in all the cases, according to the nature of the shear instability. For (6) the matter is much simpler, and according to a vanishing mean flow of the wave, we have taken $\psi(0) = \psi(\infty) = 0$.

## 3. Analytical Estimates

In this section the classical energy analysis of the Drazin and Howard semicircle theorem [*Drazin and Reid*, 1981] will be extended to allow for a free upper surface. In addition, an analytical expression for the phase speed of neutral vorticity waves will be given. To this end, let us multiply (5) by $\bar{\eta}$ ($\bar{}$ means complex conjugate) and integrate by parts. We easily obtain the energy identity

$$\int_{x_1}^{x_2} \frac{gH}{(V - c)^2}|\eta_x|^2 dx - k^2\int_{x_1}^{x_2}\left(1 - \frac{gH}{(V - c)^2}\right)|\eta|^2 dx = \frac{gH}{(V - c)^2}\bar{\eta}\eta_x\Big|_{x_1}^{x_2} \qquad (7)$$

with $x_1$ and $x_2$ being any two points in $[0, \infty)$ and $c$ being the complex phase speed.

Let us first assume $c_i \neq 0$. Then $V(x) - c$ does not vanish, the integrand in (7) is bounded, and we can perform the integral in the whole $[0, \infty)$ interval. As $H(0) = 0$, assuming that $H\bar{\eta}\eta_x(\infty) = 0$, the right-hand side of (7) with $x_1 = 0$ and $x_2 = \infty$ vanishes. Then, by taking real and imaginary part in (7), we obtain

$$\int_0^\infty \frac{(V - c_r)^2 + c_i^2}{D^2} Q\, dx = k^2\int_0^\infty |\eta|^2\, dx \qquad (8)$$

$$c_i\int_0^\infty \frac{V - c_r}{D^2} Q\, dx = 0 \qquad (9)$$

where

$$Q(x) = gH(|\eta_x|^2 + k^2|\eta|^2),\ D(x)^2 = ((V - c_r)^2 + c_i^2)^2 + 4c_i^2(V - c_r)^2$$

Owing to (9), since $c_i \neq 0$ and $Q > 0$, $V(x) - c_r$ must vanish somewhere, and then the Rayleigh condition

$$V_{\min} < c_r < V_{\max} \qquad (10)$$

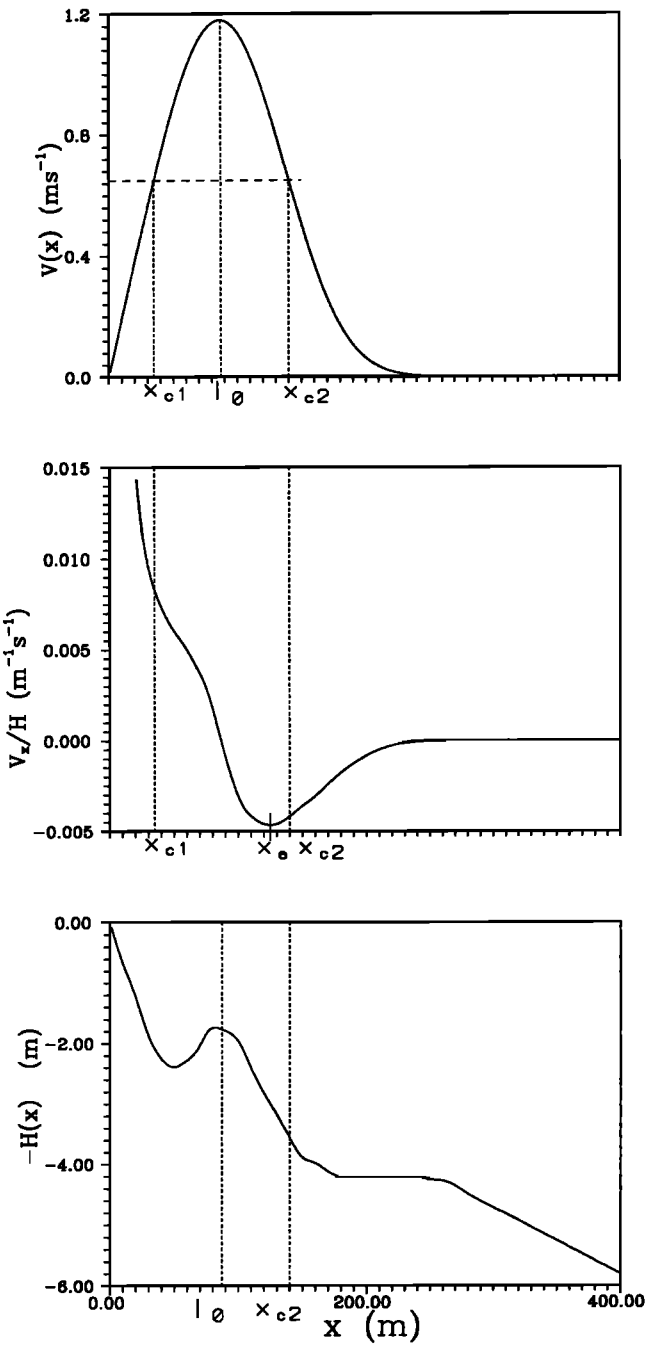


**Figure 1.** Mean flow profile according to (14) with $n = 3$, $a = 0.019\ s^{-1}$, and $b = 0.008\ m^{-1}$; bathymetry from Duck, North Carolina [after *Bowen and Holman*, 1989], and consequent potential vorticity profile. The critical locations $x_{c1}$ and $x_{c2}$ for an arbitrary phase speed $c$ are pointed out.

follows. Now we may continue by following the classical method of proof of the semicircle theorem for the Rayleigh equation. So, from

$$\int_0^\infty \frac{Q}{D^2}(V - V_{\min})(V - V_{\max})\,dx \le 0$$

and taking into account (8) and (9), after some standard calculations we obtain

$$\left(c_r - \frac{V_{\min} + V_{\max}}{2}\right)^2 - c_i^2 \le \left(\frac{V_{\max} - V_{\min}}{2}\right)^2 \quad (11)$$

We therefore obtain a region in the complex $c$ plane bounded by a hyperbola instead of the inner part of a circle that one can obtain for the Rayleigh equation or for (6) [see *Dodd and Thornton*, 1990]. Thus because (11) is less restrictive than (10), the only limitation we can find on the $c$ spectrum by this method is the Rayleigh condition (equation (10)). Obviously, this does not imply that stronger estimates could not be obtained by other methods. In fact, for the cases studied, the computed spectra verify the semicircle bound.

Let us now consider neutral waves, that is, $c_i = 0$. Let us assume a structure of the mean flow like that shown in Figure 1, with the peak located at $l_0$, $V(l_0) = V_{\max}$, and where for $V_{\min} = 0 < c < V_{\max}$ the relative velocity $(V(x) - c$ has only two simple roots, $x_{c1} < x_{c2}$. Let us define

$$p(x) = \frac{d}{dx}\left(\frac{V_x}{H}\right)$$

where $V_x/H$ is the potential vorticity. We suppose a structure of the bathymetry and the potential vorticity like that in Figure 1, where potential vorticity is a decreasing cross-shore function at the first root, yielding to $p(x_{c1}) \neq 0$, and where $H(x) \ge H(l_0)$ for $x > x_{c2}$. Finally, if $F = [V(x)/(gH(x))^{1/2}]_{\max}$ is the maximum local Froude number of the mean flow, $F < 1$ is assumed. Under such a hypothesis, if $p(x_{c2}) \neq 0$ and because the velocity field must be bounded, it was shown in a previous paper [*Falqués and Iranzo*, 1992] that (5) has only solutions vanishing for $x \ge x_{c1}$. These solutions were numerically computed and were shown to be edge waves. Instead, if $p(x_{c2}) = 0$, there may be a second class of solutions extending beyond $x_{c1}$ and behaving like

$$\eta(x) = b_0\left[1 - \frac{k^2}{2}(x - x_{c2})^2 + \cdots\right] \quad (12)$$

near $x_{c2}$. Then, if the potential vorticity has an extremum at $x_a$ in the sea face of the velocity profile (see Figure 1), we have $p(x_a) = 0$, and there can therefore be a solution of the second class with

$$c = c_{ne} = V(x_a) \quad (13)$$

This solution is a neutral vorticity wave and will be numerically computed in section 5. Moreover, we will see that though (13) holds only for neutral waves, it gives rise to an estimate of the phase speed of growing modes.

## 4. Numerical Methods

### Eigenvalue Problem

The present method computes the spectrum of complex phase speeds $c = c_r + ic_i$ and the cross-shore structure of the waves for any wavenumber $k$ by transforming (3) or (6) into a linear algebraic eigenvalue problem. For inviscid flow, handling the single equation (5) would be more advantageous than dealing with system (3). However, this does not seem possible, because $c$ does not appear in (5) as a linear eigenvalue. For the computation of edge waves on a long-shore flow [*Falqués and Iranzo*, 1992], this difficulty was overcome by taking the phase speed as a velocity scale or as a parameter for the dispersion curves. But in dealing with growing vorticity waves, this treatment is not possible,

because $c$ is complex. At least for neutral vorticity waves, considering (5) in a way similar to that for edge waves would seem possible. But now another difficulty appears: since the solution extends over the whole interval $[0, \infty)$ and $c$ is real, $V(x) - c$ may vanish somewhere in the integration domain, yielding to singularities. A direct standard discretization of this equation that ignores the singularities is therefore ill-advised. Thus we have dealt with (5) only for neutral waves but by using the overshooting method. For the eigenvalue problem we have handled system (3) or (6).

To obtain an algebraic eigenvalue problem approximating (3) or (6), the first method used was a rational Chebyshev collocation scheme [*Boyd*, 1987]. This method was proved to be very efficient in several test problems [*Iranzo and Falqués*, 1992] and in computation of edge waves [*Falqués and Iranzo*, 1992]. This is so because the largest concentration of collocation nodes is at $x = 0$, and then the resolution is maximum near the shoreline and decays monotonically offshore in a way similar to that of the cross-shore structure of edge waves. On the other hand, shear instability simulation requires the highest resolution not near the shoreline but at the peak and at the sea face of the mean velocity profile. So we found a domain decomposition technique to be more efficient (fewer base functions to obtain a given error bar). The procedure is as follows. The integration domain is cut into two parts, $[0, l_1]$ and $[l_1, \infty)$. Then Chebyshev collocation is used in the finite part, and rational Chebyshev collocation is used in the infinite part. Continuity of the solution and of its first derivative is imposed at the matching point, $x = l_1$. To this end let us consider the maps from the $[0, l_1]$ and $[l_1, \infty)$ intervals into the $[-1, 1)$ one, given by

$$x = \phi_1(\zeta) = \frac{l_1}{2}(1 - \zeta) \qquad \zeta \in [-1, 1)$$

if $x \in [0, l_1]$ and by

$$x = \phi_2(\xi) = l_1 + l_2 \frac{1 + \xi}{1 - \xi} \qquad \xi \in [-1, 1)$$

if $x \in [l_1, \infty)$. Functions are expanded in each interval as

$$f(x) = \sum_{n=0}^{N_1} a_n T_n(\zeta) = \sum_{n=0}^{N_1} a_n T_n(\phi_1^{-1}(x)) \qquad 0 \le x \le l_1$$

$$f(x) = \sum_{n=0}^{N_2} b_n T_n(\xi) = \sum_{n=0}^{N_2} b_n T_n(\phi_2^{-1}(x)) \qquad l_1 \le x$$

From the Gauss-Lobatto nodes

$$\zeta_i = \cos\frac{\pi i}{N_1} \qquad i = 0 \cdots N_1$$

$$\xi_i = \cos\frac{\pi i}{N_2} \qquad i = 0 \cdots N_2$$

discretization of differential equations follows from colocation at the transformed nodes:

$$x_i = \phi_1(\zeta_i) \qquad i = 0 \cdots N_1 - 1$$

$$x_i = \phi_2(\xi_{N-i}) \qquad i = N_1 \cdots N - 1$$

where $N = N_1 + N_2$. Note that $x_0 = 0$, $x_{N_1} = l_1$, and $x_N = \infty$. The first and second derivatives at the nodes of any function $f(x)$ are computed by means of

$$\left.\frac{df(x)}{dx}\right|_{x=x_j} = \sum_{k=0}^{N_1} (D_1)_{jk} f_k \qquad j = 0 \cdots N_1$$

$$\left.\frac{df(x)}{dx}\right|_{x=x_j} = \sum_{k=N_1}^{N-1} (D_2)_{jk} f_k \qquad j = N_1 \cdots N - 1$$

$$\left.\frac{d^2f(x)}{dx^2}\right|_{x=x_j} = \sum_{k=0}^{N_1} (D_1^2)_{jk} f_k \qquad j = 0 \cdots N_1$$

$$\left.\frac{d^2f(x)}{dx^2}\right|_{x=x_j} = \sum_{k=N_1}^{N-1} (D_2^2)_{jk} f_k \qquad j = N_1 \cdots N - 1$$

where $f_k = f(x_k)$. (We are assuming that $f(x)$ vanishes at infinity, so the $x_N$ node does not have to be considered.) Owing to the chain rule, the derivative matrices are given by

$$(D_1)_{jk} = \frac{1}{\phi_1'(\zeta_j)} \bar{D}_{jk}$$

$$(D_1^2)_{jk} = \frac{1}{\phi_1'(\zeta_j)^2} (\bar{D}^2)_{jk} - \frac{\phi_1''(\zeta_j)}{\phi_1'(\zeta_j)^3} \bar{D}_{jk} \qquad j, k = 0 \cdots N_1$$

and similar expressions for the second interval (but with index shifts), $\bar{D}$ and $\bar{D}^2$ being the Chebyshev derivative operators [*Canuto et al.*, 1988]. The continuity of the solution at the matching point $x_{N_1} = l_1$ is automatically guaranteed, because only one value of the solution at this point is handled, whether it was considered to belong to $[0, l_1]$ or to $[l_1, \infty)$. On the other hand, continuity of the first derivatives must be explicitly imposed by

$$\sum_{k=0}^{N_1} (D_1)_{N_1 k} f_k - \sum_{k=N_1}^{N-1} (D_2)_{N_1 k} f_k = 0$$

replacing the differential equations at this node. In summary, at $x_0 = 0$ boundary conditions, at $x_1 \cdots x_{N_1-1}$, and at $x_{N_1+1} \cdots x_{N-1}$, we impose the differential equations, and at $x_{N_1}$, we impose the continuity conditions. The conditions at infinity, $u(\infty) = v(\infty) = \eta(\infty) = 0$, are fulfilled simply by dropping the $x_N = \infty$ node as usual in rational Chebyshev developments.

As is known, discrete approximations of eigenvalue problems may exhibit spectral pollution; that is, the appearance of spurious eigenvalues that do not converge to the correct value when the mesh density is increased [*Llobet et al.*, 1990]. Hence one has to carefully handle the computed spectrum, and some test is always a must. The numerical model was tested by application to the well-known problem of edge wave propagation on a plane sloping beach without mean flow, giving a similar accuracy to rational Chebyshev collocation [*Falqués and Iranzo*, 1992]. Another test was yielded from the stability of the results to an increasing number of base functions. In the presence of a mean current, most modes in the spectrum show large variations when $N$ is varied.

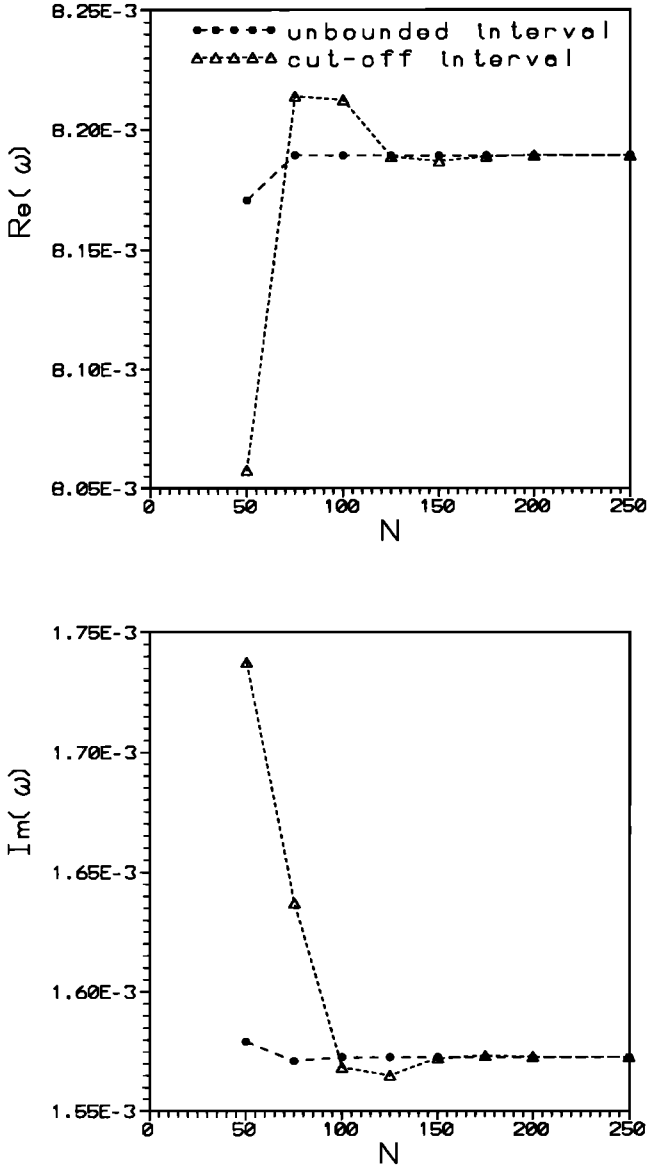


**Figure 2.** Numerical efficiency of the unbounded interval numerical method compared to the cutting-off approach.

These solutions may therefore be spurious modes. They also may correspond to true solutions of the differential equations which are poorly described by our discrete method because they have strong gradients or too many oscillations [*Iranzo and Falqués*, 1992]. Anyway, these numerical solutions cannot be considered with certainty as approximations to true solutions of the physical problem. However, we also found solutions showing stability to an increase in $N$. Some of them, with real $c$, were identified as advected edge waves, and the remaining ones, with complex conjugate eigenvalues $c = c_r \pm ic_i$, could be identified as shear waves.

The previous method addressed by *Putrevu and Svendsen* [1992] cuts off the [0, ∞) interval and thus enforces the boundary condition not at infinity but at a finite distance from the shoreline. Such an approximation is justified because the solution dies far offshore. Nevertheless, handling an interval two or more times larger than the cross-shore range of the solution is then necessary, with the result that half or more of the discretization nodes are wasted because they are located where the solution has died. Instead, rational Chebyshev expansions expend very few nodes in this zone. For this reason the present method is more efficient. In Figure 2 the complex frequency computed by the present method or by Chebyshev collocation in a finite interval (3.6 times the current width) is represented against the number of nodes $N$. We can see how the present method achieves convergence with a third to half of the nodes required by the other method. In addition, as is known [*Canuto et al.*, 1988; *Boyd*, 1989], convergence of spectral methods is faster than any power of $N$, and thus the present method is likely to require less than a third of the nodes required for the finite-difference method of Putrevu and Svendsen in order to reach a given accuracy.

### Overshooting Method

The overshooting method has been used by several authors [*Howd et al.*, 1992; *Dodd et al.*, 1992; *Falqués and Iranzo*, 1992] to solve eigenvalue problems in a semi-infinite interval $[x_a, \infty)$. It considers an initial value problem for the differential equations starting from $x_a$. Then the eigensolution is selected by enforcing the solution to die away as $x \to \infty$. We have used it in order to find neutral solutions to (5) in the $[x_a, \infty)$ interval, $x_a$ being the location of the minimum of the potential vorticity. We started at $x_a + \varepsilon$, with $\varepsilon$ being a small distance to avoid the singularity at $x_a$. As the initial condition we enforce matching with the analytic solution near $x_a$, (12), up to fourth order, where the coefficients can be seen in the work of *Falqués and Iranzo* [1992]. Finally, we pick $c$ given by (13), and then we find $k$ and $\eta(x)$ for $x \geq x_a + \varepsilon$. In this way we could accurately compute the critical wavenumber $k_{c2}$, above which there is no shear instability. The procedure is as follows. For dimensionless variables in the case of a plane sloping beach (see section 5), we choose $\varepsilon = 0.05$ and try to minimize $\eta(x_\infty)$ with $x_\infty = 6$. Then we proceed for lower values of $\varepsilon$ up to $\varepsilon = 0.001$, obtaining convergence of $k$ for $\varepsilon \to 0$. Despite that, because of numerical inaccuracies arising from the singularity at $x_a$, for very low $\varepsilon$ the solution diverges. Nevertheless, we can reasonably choose a $k_{c2}$ value within an error bar of 0.5% (see Table 1). Curiously, we found neutral shear waves only for one wavenumber, $k_{c2}$, whereas the BH model gives rise to two neutral waves for every $k$ above $k_{c2}$ and below $k_{c1}$.

## 5. Instability Curves and Dispersion Relations

For the numerical simulation we considered several cases. The cross-shore profile of the mean longshore flow was chosen to be in all cases

$$V(x) = ax \exp\left[-(bx)^n\right] \tag{14}$$

with a peak given by

$$V_{\max} = \frac{a}{b}(en)^{-1/n}$$

located at

$$l_0 = (n)^{-1/n} b^{-1}$$

and a maximum backshear of magnitude given by

$$f_s = na \exp[-(n+1)/n]$$

so that for fixed $a$, $b$ or for fixed $l_0$, $V_{max}$, the maximum backshear $f_s$ can be increased by increasing $n$. According to BH, this profile with $n = 3$ may be quite realistic in the surf zone. Regarding the bathymetry we considered several options.

*Case A: Plane sloping beach, $H(x) = \beta x$.* In order to make an exploration for any beach slope $\beta$ for any flow with the form (14) and $n = 3$, equations (3) were scaled by taking $L = \beta/b$ and $T = \beta/a$ as length and time scales. The gravity acceleration $g$ was then replaced by the dimensionless parameter

$$g^* = \frac{\beta b g}{a^2} = \frac{(2en)^{-1/n}}{F^2}$$

where $F = [|V(x)|/(gH(x))^{1/2}]_{max}$ is the maximum Froude number of the mean flow. For $n = 3$, we have $g^* = 0.394/F^2$. The wavenumber and the (complex) phase speed were replaced by the dimensionless magnitudes $k/b$ and $bc/a$. According to BH, the natural scaling of shear instability is provided by the maximum shear at the seaward face of the mean current profile $f_s$, the width of the longshore current, and the peak longshore current $V_{max}$. Then the former scales can be related to the latter by $T = 0.7908\beta/f_s$ and $L = 1.442\beta l_0$. The velocity scaling is provided by $a/b = 2.013V_{max}$. Note that the dissipative parameters are replaced by

$$\varepsilon^* = \frac{b^2}{a}\varepsilon = 0.380\frac{\varepsilon}{f_s l_0^2} \qquad \mu^* = \frac{g}{\beta C^2}$$

*Case B: Flat bottom.* In order to explore the influence of different current profiles, we took a flat-bottom beach, $H(x) = H_0$, and the velocity profile given by (14) with $V_{max} = 1.2$ m s$^{-1}$ and $l_0 = 90$ m for several $n$.

*Case C: Exponential profile with finite depth at infinity $H_\infty$ and a slope at the shoreline $\beta$:$H(x) = H_\infty[1 - \exp(-\beta x/H_\infty)]$.* For this depth profile we considered a fixed flow given by (14) with $n = 3$ and a peak longshore current $V_{max} = 1.2$ m s$^{-1}$ located at $l_0 = 90$ m.

*Case D: Barred beach.* In order to use a realistic bathymetry, we took an $H(x)$ function interpolated from field data reported by BH and belonging to a barred beach (Duck, North Carolina; see Figure 1). The velocity profile was chosen as the latter case, so its peak is roughly 5 m offshore of the bar.

**Table 1.** Computation of Cutoff Wavenumber $k_{c2}$ by Using the Overshooting Method

| $\varepsilon$ | $L$ | $k$ |
|---|---|---|
| 0.00001 | 4.0 | 2.22238941 |
| 0.0001 | 4.0 | 2.65731100 |
| 0.0005 | 4.0 | 2.66151479 |
| 0.0007 | 4.0 | 2.66161364 |
| 0.001 | 6.0 | 2.66168046 |
| 0.003 | 6.0 | 2.66187429 |
| 0.005 | 4.0 | 2.66204656 |
| 0.005 | 6.0 | 2.66204651 |
| 0.006 | 6.0 | 2.66213656 |
| 0.007 | 6.0 | 2.66222981 |
| 0.009 | 6.0 | 2.66242635 |
| 0.01 | 6.0 | 2.66252990 |
| 0.02 | 6.0 | 2.66376708 |
| 0.03 | 6.0 | 2.66539852 |
| 0.04 | 6.0 | 2.66746126 |
| 0.05 | 6.0 | 2.66999164 |

Plane sloping beach, inviscid flow, $F = 0.14$.

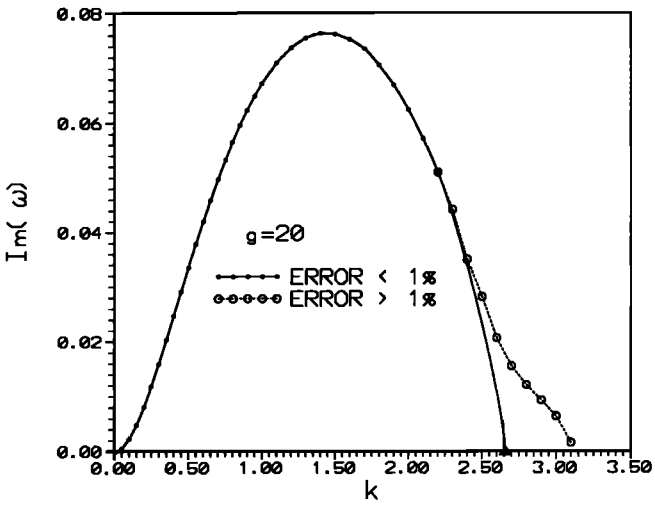


**Figure 3.** Typical instability curve for a plane sloping beach with inviscid flow. Near the transition for the highest unstable wavenumber, there is a lack of numerical accuracy, so the curve computed by the eigenproblem (dashed curve) is no longer reliable. The solid curve has been obtained by interpolation between the last reasonably accurate $(k, \omega_I)$ point and $(k_{c2}, 0)$, with $k_{c2}$ being obtained by the overshooting method.

For each beach profile, computations were worked out with or without the rigid-lid assumption by solving (6) or (3). Most of the calculations were carried out for inviscid flow, that is, $\varepsilon = 0$ and $g/C^2 = 0$. However, in order to find the influence of the bottom friction, we made some trials with a Chezy coefficient $C$ between 30 to 100 m$^{1/2}$ s$^{-1}$, which according to *van Rijn* [1987] are reasonable values for real beaches. Also, in order to find the influence of turbulent dissipation, we considered the simplest case of a homogeneous and isotrope eddy viscosity. Again, following van Rijn, reasonable values of $\varepsilon$ of about 0.1 to 1 m$^2$ s$^{-1}$ were taken.

### Case A

We performed an exploration in the case of a rigid lid and in the case of a free surface for $g^* = 0.5, 1, 20, 100$, which correspond to $F = 0.89, 0.63, 0.14, 0.063$. The patterns we found for these cases were similar. Among the computed complex eigenvalues for each $k$ there are only two conjugate eigenvalues, $c = c_r \pm ic_i$, that converge when $N$ increases. In the search for growing modes, only the solution with $c_i > 0$ was taken into account. Comparing its order of magnitude and the spatial structure of the corresponding eigenmode with those arising from the analysis of BH revealed that this eigensolution was a vorticity wave. The growth rate $\omega_i$ against wavenumber $k$ curves without dissipation start from the origin (0, 0), increase up to an absolute maximum at $k_M$, and then decrease up to $k_{c2}$, where $\omega_i = 0$ and the instability ceases (see Figure 3). The $k_M$ wavenumber where $\omega_i$

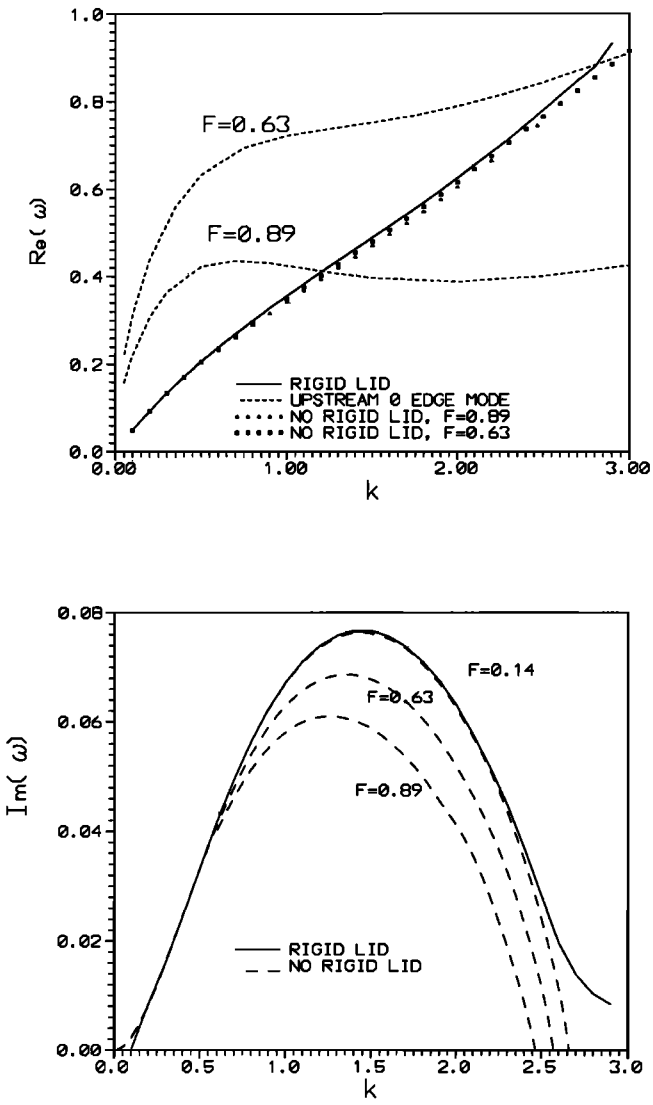


**Figure 4.** (*a*) Dispersion lines and (*b*) instability curves for inviscid flow and free surface on a plane sloping beach for several Froude numbers ($F$). The corresponding rigid-lid computations are also shown. The dispersion line of the 0th upstream edge mode is plotted in Figure 4*a* to show that for high Froude number the frequencies of shear waves and gravity waves may become mixed.

reaches its absolute maximum, corresponding therefore to the fastest growing mode and being expected as the most easily seen in natural beaches, is called the dominant wavenumber. The critical wavenumber $k_{c2}$ is the cutoff one above which there is no shear instability. This pattern is qualitatively similar to that found by BH and *Dodd and Thornton* [1990], except that for the inviscid flow case we do not find a lower critical wavenumber $k_{c1} > 0$ below which there is no shear instability. Values of the discretization parameters $l_1$ and $l_2$ that were roughly similar to the width of the mean current profile were picked. Some trials were made, and we finally preferred to include the region of the main variation of solutions in the finite interval, leaving for the semi-infinite interval only the far offshore monotone decay to zero. So, for instance, for a plane beach with peak mean velocity at $x = 0.69$ and width current profile of about 1.69 (approximately, from Figure 1; in fact the current width would be infinite), we took $l_1 = 1.2$, $l_2 = 1$, $N_1 = 100$, and $N_2 = 20$, giving rise to a high resolution at the sea face of the current profile. Usually, the numerical accuracy was very good except near $k_{c2}$ or near $k_{c1} = 0$. For example, with a plane sloping beach, $k = 0.01\ \text{m}^{-1}$, $l_1 = 160$ m, $l_2 = 60$ m, $N_1 = 50$, and $N_2 = 20$, we get an error bar of less than 0.002%. Instead, near $k_{c2}$ the accuracy strongly decreases, and before $\omega_i$ has fallen to zero, the true eigenmode can hardly be identified in the spectrum, resulting in a rather irregular, probably spurious behavior of the instability curve near $k_{c2}$ (see Figure 3). Thus the central parts of the instability curves were usually computed with $N = 70$, and the extrema were computed with $N = 120$. For the barred beach case, because of the sharp variations in $H(x)$, a greater resolution was needed (the same as for edge waves [*Falqués and Iranzo*, 1992]), and the whole instability curve was computed with $N = 120$.

The dispersion relations are quite linear (Figure 4), showing little dispersion, and the phase speed is about 0.5 to $0.7V_{\max}$ for $k$ near $k_M$. For very low wavenumbers, the phase speed tends in all cases to $V_{\max}$. It appears that though we are dealing with growing modes, the phase speed for neutral waves, (13), gives rise to a good approximation within 4% for the dominant wavenumber in this case (plane beach with flow profile given by (14)).

As we can see in Figure 4, decreasing the Froude number causes the instability curves to lift up and tend to the rigid-lid curve (except near $k_{c1}$ or $k_{c2}$, where some differences may arise). So, it becomes apparent that the rigid-lid assumption tends to overestimate the instability. Nevertheless, for reasonably strong currents with $F$ of 0.14 to 0.63, the error in $\omega_i$ is small, between +0.5% and +12%. The rigid-lid assumption also tends to overestimate the frequency but by a smaller amount of +0.1% to +2% for $F$ between 0.14 and 0.63 (see Table 2). For $F \leq 0.63$, the dominant wavenumber is $k_M = 1.44b$, with a frequency of $\omega_r = 0.4717a$ and a growth rate of $\omega_i = 0.0764a$. This gives rise to a dominant wavelength of $\lambda_M = 6.29l_0$, a frequency of $\omega_r = 0.596f_s$, a growth rate of $\omega_i = 0.0966f_s$, and a phase speed of $c_r = 0.659V_{\max}$. Assuming a mean current width of about $2.6l_0$, the dominant wavelength is 2.5 times this width, in rough agreement with the BH model.

The cutoff wavenumber $k_{c2}$ was computed by means of the overshooting method as outlined in section 4 (see Table 1). For $F = 0.14$, we found a cutoff wavelength of $\lambda_{c2} = 3.41l_0$, that is, about 1.35 times the mean current width. Hence, in Figure 4 we have drawn the instability curves, replacing their upper (spurious) parts with an interpolation between the last $(k, \omega_i)$ reasonably accurate point and $(k_{c2}, 0)$ (see Figure 3).

The influence of eddy viscosity on the dispersion lines and growth rate curves is shown in Figures 5*a* and 5*b* for $\varepsilon^* = 0.005$. For $V_{\max} \sim 1.2$ m s$^{-1}$ and $l_0 \sim 90$ m, this would

**Table 2.** Errors Due to the Rigid-Lid Assumption

| $F$ | $w_r$, % | $w_i$, % |
|---|---|---|
| 0.14 | +0.1 | +0.5 |
| 0.63 | +2 | +12 |
| 0.89 | +4 | +28 |

Plane sloping beach, inviscid flow.

correspond to an eddy viscosity of $\varepsilon \sim 1.6\ m^2\ s^{-1}$, which is quite strong but still realistic. Similarly, the effect of bottom friction is shown for $\mu^* = 0.078$. For a bottom slope of $\beta = 0.05$ $\mu^*$ corresponds to a Chezy coefficient of $C = 50\ m^{1/2}\ s^{-1}$, which is also in the range of reasonable values. In both cases we found a significant decrease in the growth rates but little variation in the dominant wavenumber. We also see that taking into account bottom friction as well as eddy viscosity results in the existence of a critical wavenumber $k_{c1} > 0$, below which there is no instability. Moreover, as expected, the whole wavenumber range of the instability is reduced. The presence of dissipation also produces a small decrease in frequencies. For these values of the parameters, eddy viscosity yields a decrease of about 9% in the phase speed, and bottom friction yields a decrease of about 4%. As we can see in Figure 6, by increasing eddy viscosity the instability can be removed. This occurs for $\varepsilon^* = 0.008$. Then, according to the scaling introduced, a stability condition

$$\varepsilon > 0.021 f_s l_0^2 \tag{15}$$

follows. Similarly, concerning bottom friction, the transition is obtained at $\mu^* = 0.14$. Therefore the basic flow will be stable when

$$\frac{1}{\beta}\frac{g}{C^2} > 0.14 \tag{16}$$

All of these calculations have been performed for a plane beach with the flow profile given by (14) and for $F = 0.14$. However, the results are expected to hold as an estimate for any reasonable Froude number, because as we have seen, for moderate Froude numbers the instability shows almost no dependence on $F$.

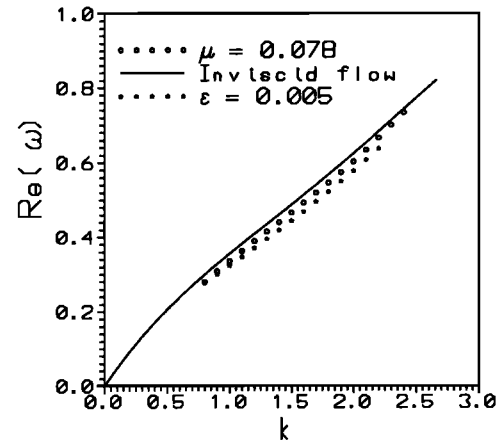


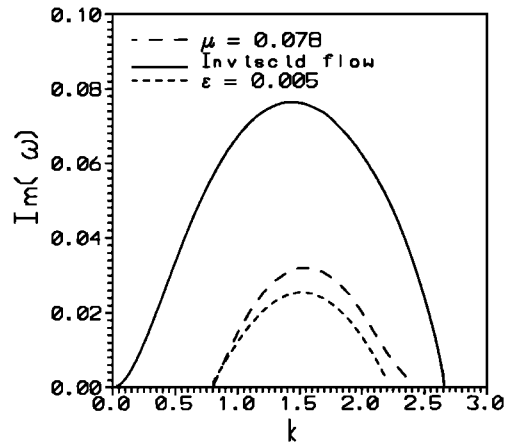


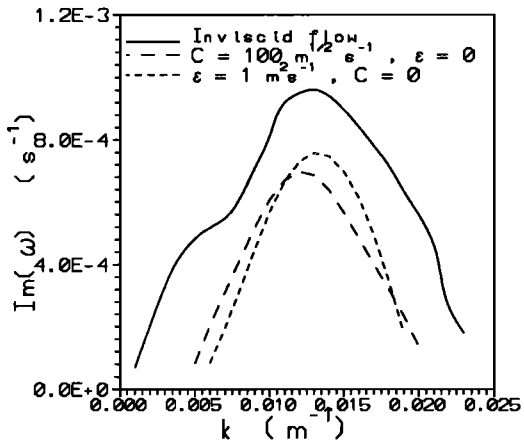


**Figure 5.** Influence of dissipation (a) on the dispersion line and (b) on the instability curve for a plane sloping beach with $F = 0.14$ (variables and parameters are dimensionless according to section 5), and (c) the influence on the instability curve for a barred beach and for the flow given by (14) with $n = 3$, $V_{max} = 1.2\ m\ s^{-1}$, and $l_0 = 90$ m is shown in Figure 5c.

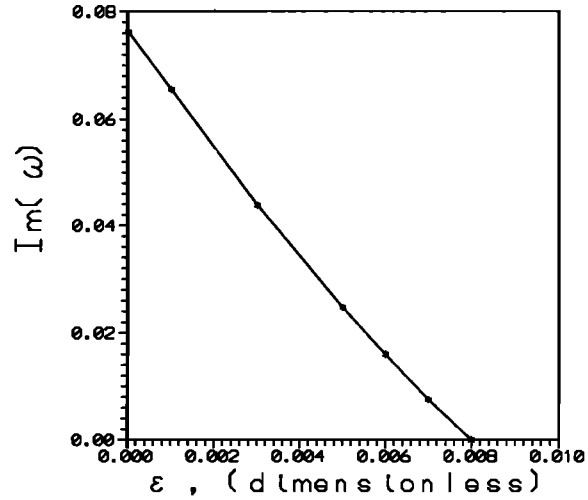


**Figure 6.** Influence of a constant eddy viscosity on the growth rate of the instability. Plane sloping beach, free surface, $F = 0.14$. Viscosity has been scaled to $a/b^2$.

## Case B

An exploration for $n = 2, 3, 4, 5$ with a rigid lid has been carried out. Figure 7 shows the flow and the potential vorticity profiles corresponding to these $n$ exponents. The instability curves for $n = 3, 4, 5$ displayed in Figure 8 show two relative maxima at $k_{M1}$ and $k_{M2}$, with $k_{M1} < k_{M2}$. The second maximum is the absolute one; it has an important increase with $n$, showing a quite linear dependence of $f_s$, whereas the first maximum has little variation with $n$. We found maximum growth rates of $0.12 f_s$, $0.14 f_s$, and $0.15 f_s$ for $n = 3, 4, 5$, respectively. The dominant wavenumber

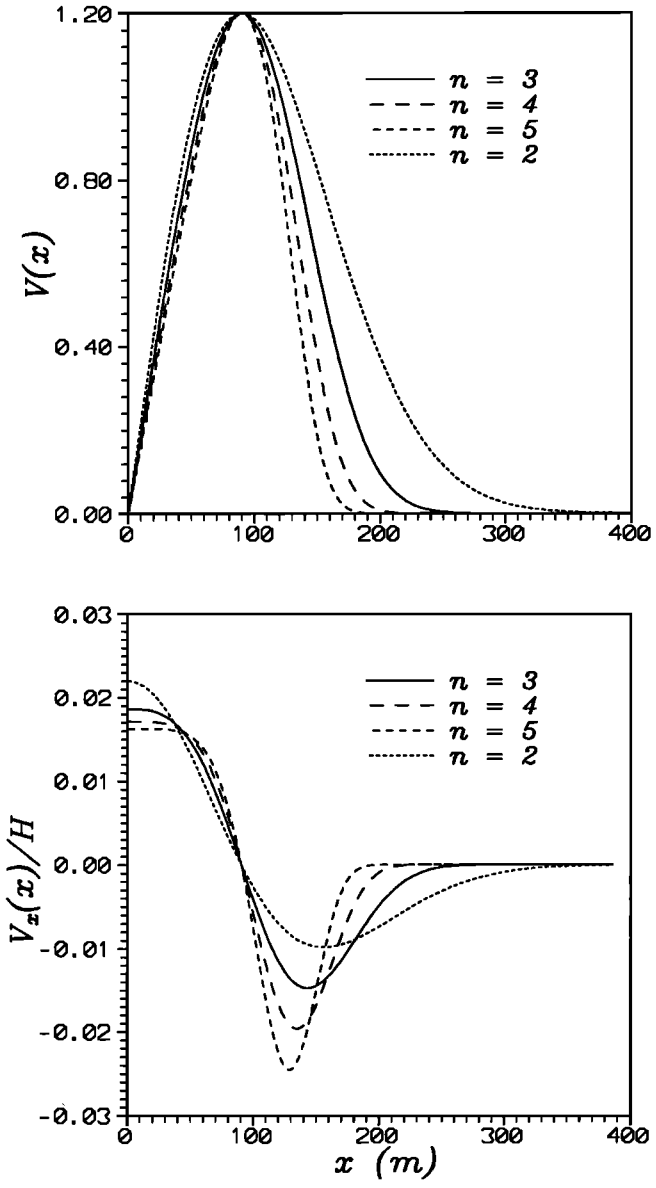


**Figure 7.** Mean flow and potential vorticity profiles for a flat-bottom beach and for some $n$ exponents, with the same current peak ($V_{max}$ = 1.2 m s$^{-1}$) located at the same place ($l_0$ = 90 m).

shows a gentle increase with $n$ according to a quite linear relation between $\lambda_{M2}$ and the current width given by $\lambda_{M2}/l \sim 1.7$–$1.8$. On the other hand, as can be seen in Figure 8, for $n = 2$ there is only one maximum, with $\lambda_M = 3.9l$ and $\omega_i = 0.08f_s$. Some calculations with $n = 1$ showed that in this case there is also just one maximum, and for high wavenumbers the instability curve falls rapidly without the kink present in the $n = 2$ case. All the curves corresponding to any $n$ exponent tend to coincide for low wavenumbers, showing that the details in the flow profile become unimportant for very long waves. In addition, some calculations without rigid lid were made for $n = 3$ and $F = 0.14$. Thus the validity of the rigid-lid assumption for the low Froude number found in case A was corroborated.

### Case C

In order to make a comparison with the case of barred beach, we took $H_\infty$ = 4.5 m and a slope at the shoreline of $\beta = 0.05$, similar to the real topography but without the bar. The instability curve, with a maximum growth rate of $\omega_i = 0.099f_s$, can be seen in Figure 10*b*. This depth profile with $H_\infty$ = 1 m fixed and with several $\beta$ was also used in order to simulate the transition from a flat bottom ($\beta = \infty$) to a nearly plane slope at the peak of the current profile ($\beta \sim 0.01$). As we can see in Figure 9, for high slope at the shoreline $\beta$ = 0.5, 0.19, we found a curve very similar to that for a flat bottom, showing two maxima. On the other hand, when $\beta$ decreases, the instability curves tend toward those of a plane sloping beach, with only one maximum. This can be seen for $\beta = 0.02$, for example. For intermediate values the curve shows an inflexion similar to that in the barred beach case (see Figure 10*b* and the curve corresponding to $\beta = 0.1$ in Figure 9).

### Case D

Now we will compare the results of the direct numerical simulation of a barred beach quoted above with the results of other available approaches. First, if we want to make a comparison with the BH model, we must define $V_{max}$, the current width $l$, and $\delta = l_0/l$. From Figure 1 we see that reasonable values may be $V_{max}$ = 1.2 m s$^{-1}$, $l$ = 220 m, and $\delta = 0.39$. The instability curves for the three depth profiles quoted above for cases A and B and for the BH model are displayed in Figure 10*b*. For the barred beach we find $\lambda_M = 2.20l$, whereas the other approaches give rise to somewhat larger dominant wavelengths of nearly $\lambda_M \simeq 2.60l$. We also see that the growth rates are of the same order: $\omega_i = 0.063f_s$ for a barred beach, $\omega_i = 0.086f_s$ for a plane beach, and $\omega_i = 0.088f_s$ for BH. We see that the dominant wavenumber for a barred beach and a free surface (case C) falls between

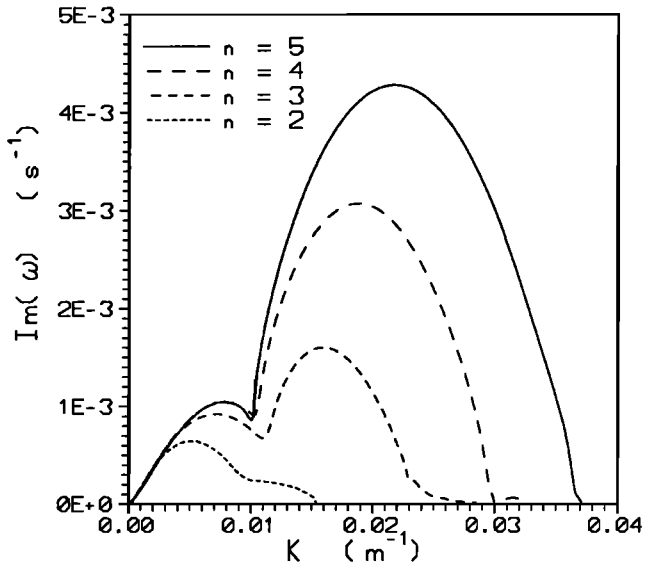


**Figure 8.** Instability curves for several $n$ exponents, with $V_{max}$ = 1.2 m s$^{-1}$ and $l_0$ = 90 m, assuming a flat bottom, rigid lid, and inviscid flow. For $n \geq 3$ we can see a fairly linear relationship between the maximum growth rate and the maximum backshear and between the dominant wavelength and the mean current width.

the two maxima appearing for a flat bottom (case B). It is also apparent that the maximum growth rate for case C is similar to the secondary maximum in case B and considerably lower than the absolute maximum. Figure 10*a* displays the dispersion relations. We see that all the curves for the flow given by (14) are quite close together and considerably higher than the BH curve. Intriguingly, the former curves tend to coincide with one branch of the BH curve and with the straight line $\omega_r = c_{ne}k$ for low wavenumbers, and for $k \to 0$ we have in all cases $c_r \to V_{max}$. Figure 11*a* displays the phase speeds. For the dominant eigensolution we find $c_r = 0.46V_{max}$ for case B, $c_r = 0.55V_{max}$ for case C, and $c_r = 0.63V_{max}$ for case A, whereas for BH we had a lower phase speed $c_r = 0.30V_{max}$. The analytical expression (13) gives a higher value, $c_{ne} = 0.73V_{max}$.

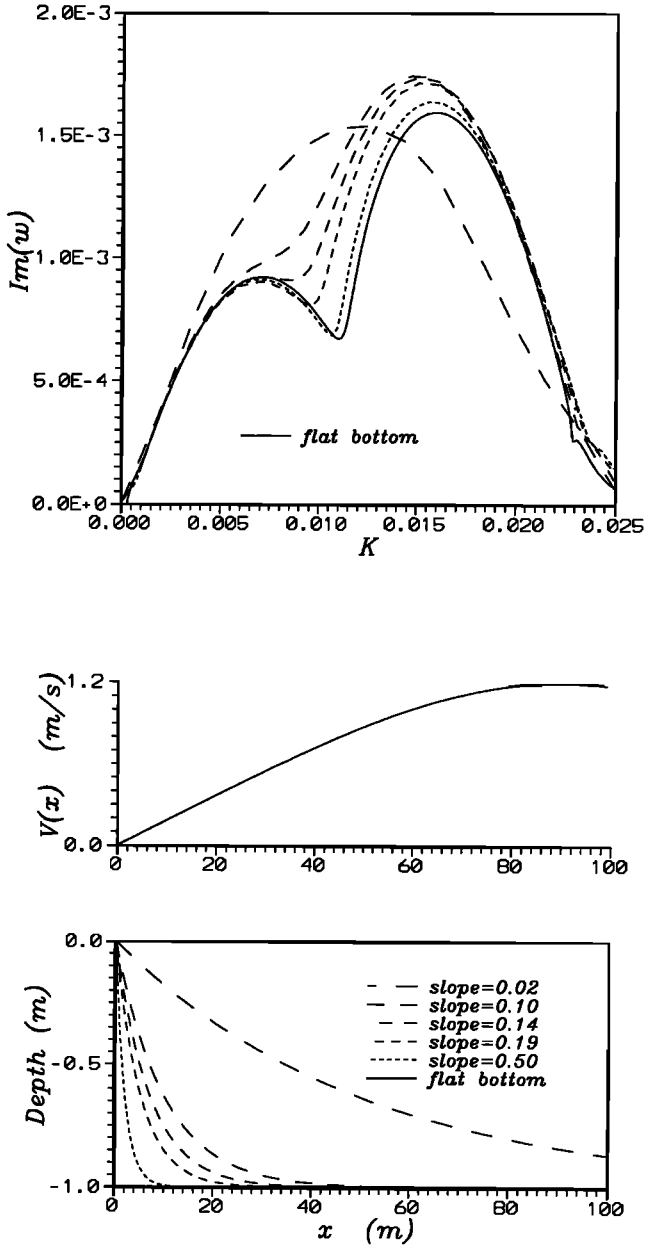


**Figure 9.** Influence of flatness on the appearance of a secondary maximum in the instability curve. Inviscid flow, $n = 3$, $V_{max} = 1.2$ m s$^{-1}$, and $l_0 = 90$ m. Exponential depth profiles for a number of slopes at the shoreline.

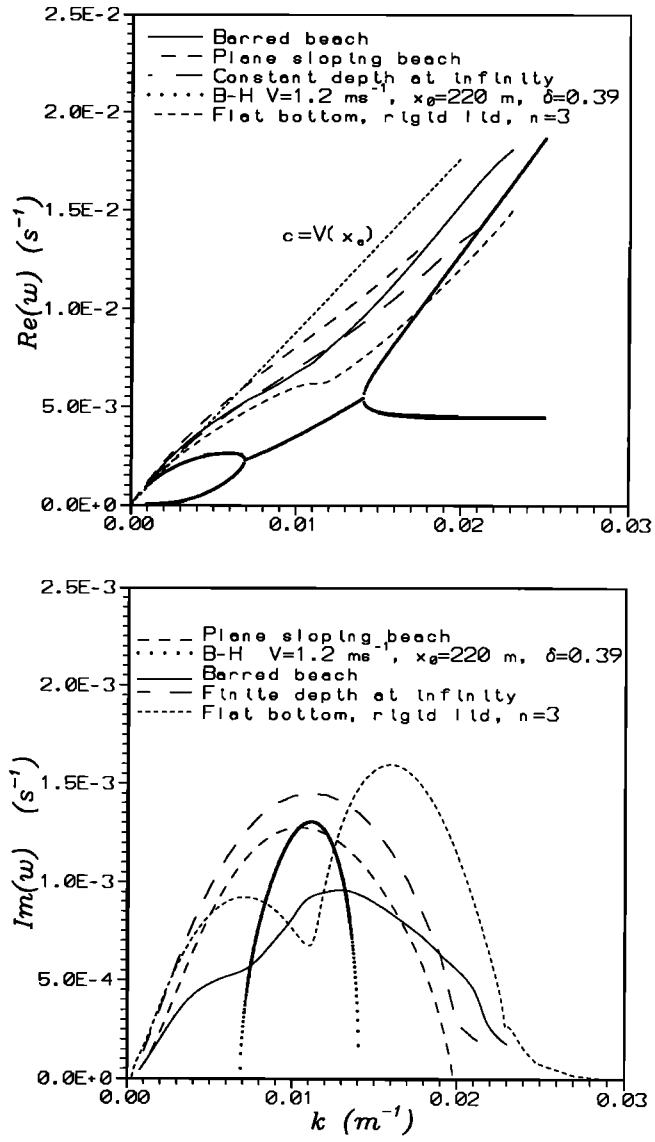


**Figure 10.** (*a*) Dispersion curves and (*b*) instability curves for inviscid flow on a barred beach in comparison with other depth profiles. The mean flow profile is that shown in Figure 9. In order to compare with *Bowen and Holman* [1989] (B-H), a finite mean current width $x_0 \simeq 220$ m has been assumed, leading to $\delta \simeq 0.39$. The estimate based on neutral modes, which according to (13) leads to $\omega_r = V(x_a)k$, has also been plotted in Figure 10*a*.

The influence of dissipation on growth rates for a barred beach is shown in Figure 5*c* for a Chezy coefficient of $C = 100$ m$^{1/2}$ s$^{-1}$ or an eddy viscosity of $\varepsilon = 1$ m$^2$ s$^{-1}$. Again, we see that dissipation does not have a great effect on $k_M$. In this case, if eddy viscosity increases, the basic flow reaches stability for $\varepsilon = 2.4$ m$^2$ s$^{-1}$, almost the same as for a plane beach (case A) with $l_0 = 90$ m and $f_s = 0.015$ s$^{-1}$. Therefore the estimate given by (15) appears to be fairly independent of the beach profile. If the Chezy coefficient is lowered, the flow reaches stability at $C = 52$ m$^{1/2}$ s$^{-1}$. According to (16), this would correspond to a plane beach

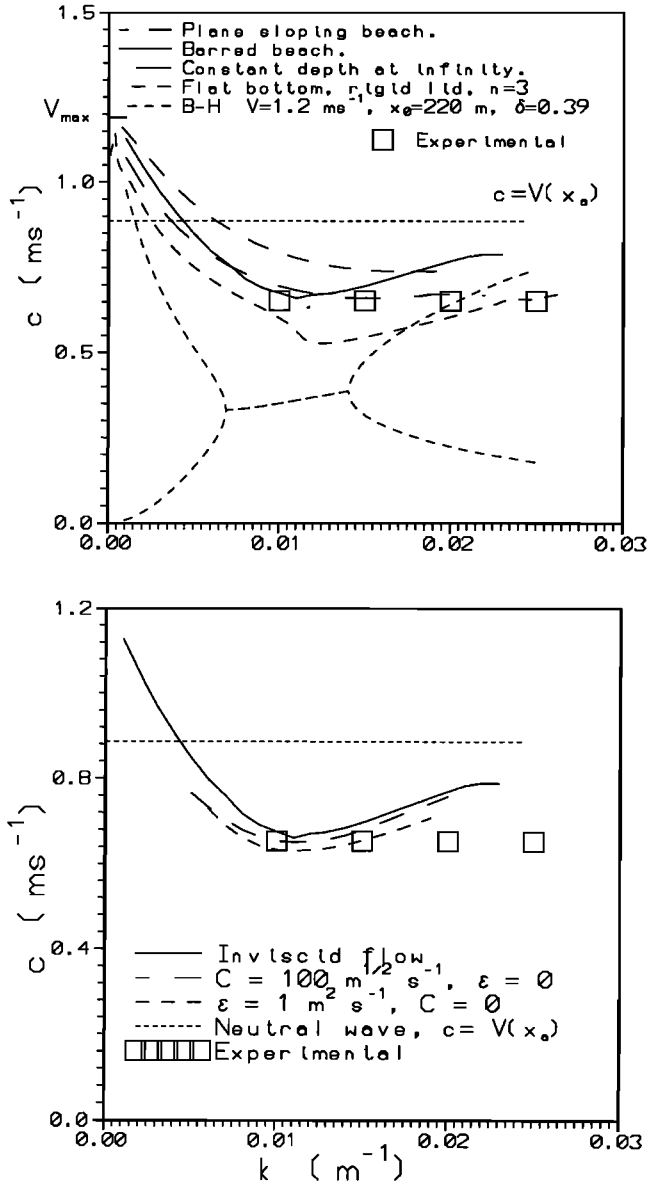


**Figure 11.** (*a*) Phase speeds of computed vorticity waves on a barred beach for inviscid flow compared with results by *Bowen and Holman* [1989] (B-H) and experimental data from work by *Oltman-Shay et al.* [1989]. The comparison with field data is difficult because the current peak value is not available, and only the mean current measure at the trough of the longshore bar was reported. In spite of this, by means of a reasonable estimate of $V_{max}$ we can see a good agreement between the experimental phase speed and the computed one. (*b*) Influence of dissipation on the phase speed.

with slope $\beta = 0.03$, which could be considered a mean slope of this barred beach. So, this stability condition could also be considered an estimate for nonplanar beaches by taking $\beta$ to be something like an overall mean slope. Finally, in Figure 11*b* we can see how dissipation results in a small phase speed decrease of about 6% or less. Note also that the effect of eddy viscosity on frequencies is, similarly to the effect on a plane beach, more important than the effect of bottom friction.

For a barred beach, the instability curve was computed with or without the rigid-lid assumption, with the result that the difference between the two computations was quite small (see Figure 12). Note that in this case the maximum Froude number is $F = 0.29$.

## 6. Spatial Structure of the Waves

The spatial structure of the waves is obtained from the eigenfunctions of (3). First, Figures 13, 14, and 15 show the real and imaginary components of $(u(x), v(x), \eta(x))$ for plane sloping topography with $F = 0.14$ and for three wavenumbers. We took $N = 120$ base functions, and the nodes were marked in order to point out the quality of the discretization. Every eigenfunction was scaled so that max $\{u_r(x), u_i(x), v_r(x), v_i(x)\} = 1$, and we see that this maximum velocity is always reached by the longshore velocity $v$. It appears that $\eta(x)$ is quite smooth, but the velocities can have strong gradients. This appears dramatically for $k = 2.4$ near the cutoff wavenumber $k_{c2}$, where internal boundary layers clearly arise. Obviously, this is the reason for the poor numerical accuracy obtained for this wavelength. In Figure 14 we can see how singularities appear for $x = x_{c1}$ and $x = x_{c2}$ that are clearly due to the fact that when $c_i \sim 0$, $V(x) - c$ almost vanishes at $x_c$ such that $V(x_c) = c_r$. For the dominant wavenumber and higher wavenumbers, the perturbation is bounded between the shoreline and 1.4 to 1.7 times the mean current width. For low wavenumbers, $k = 0.1$, the longshore velocity $v$ is located roughly on the width of the mean flow profile, but the cross-shore velocity $u$ and the surface elevation extend farther offshore, beyond 2.2 times this width. We see that a typical peak free-surface elevation is 0.006. Then, according to the scaling made for a plane beach, we have $\eta \sim 0.006\beta v/a$, and assuming $a \sim 0.019\ s^{-1}$, $\beta \sim 0.05$, and $v \sim 30\ cm\ s^{-1}$, we find that $\eta \sim 0.5$ cm.

The entire spatial structure of the wave is easily obtained by making

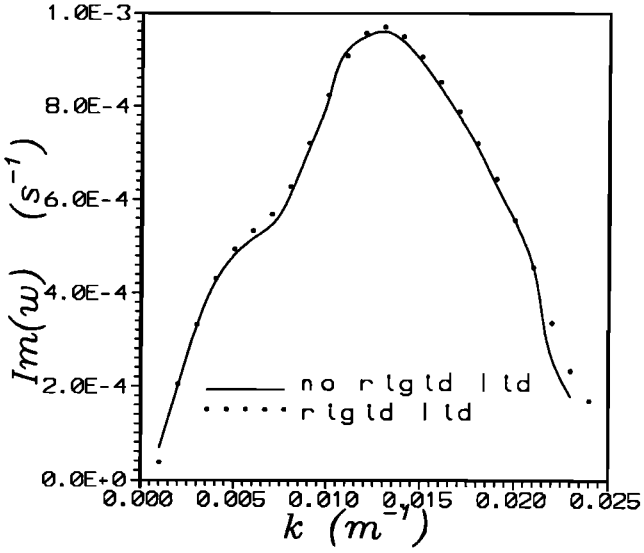


**Figure 12.** Influence of the rigid lid on the instability curve for a barred beach with inviscid flow. For these flow parameters (Figure 9) and for this bathymetry, the Froude number is $F = 0.29$.

$$f(x, y) = Re[(f_r(x) + if_i(x))e^{iky}] = (f_r(x)^2 + f_i(x)^2)^{1/2} \cos(ky + \theta(x))$$

where $f(x, y)$ is any of the functions $(u, v, \eta)$, and

$$\theta = \tan^{-1}(f_i/f_r)$$

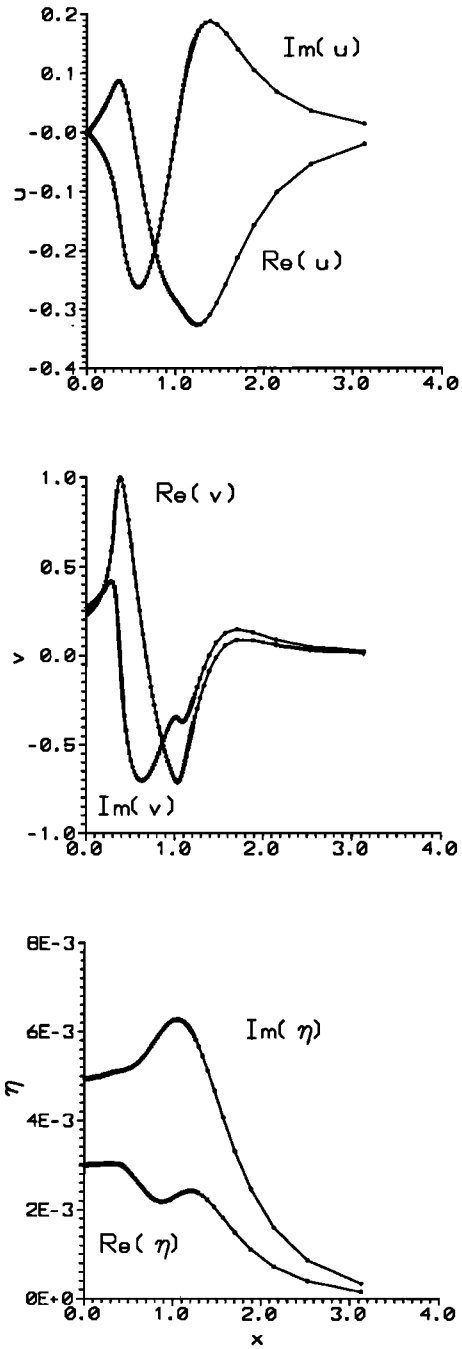


**Figure 13.** Eigensolutions of (3) for inviscid flow on a plane sloping beach with $F = 0.14$ and $k = 1.4$ near the dominant wavenumber. The calculation was made with $N = 120$. Note the suitable distribution of the collocation nodes, with a high concentration where the fastest variations of the solution occur and a lower concentration where the solution monotonically falls to zero.

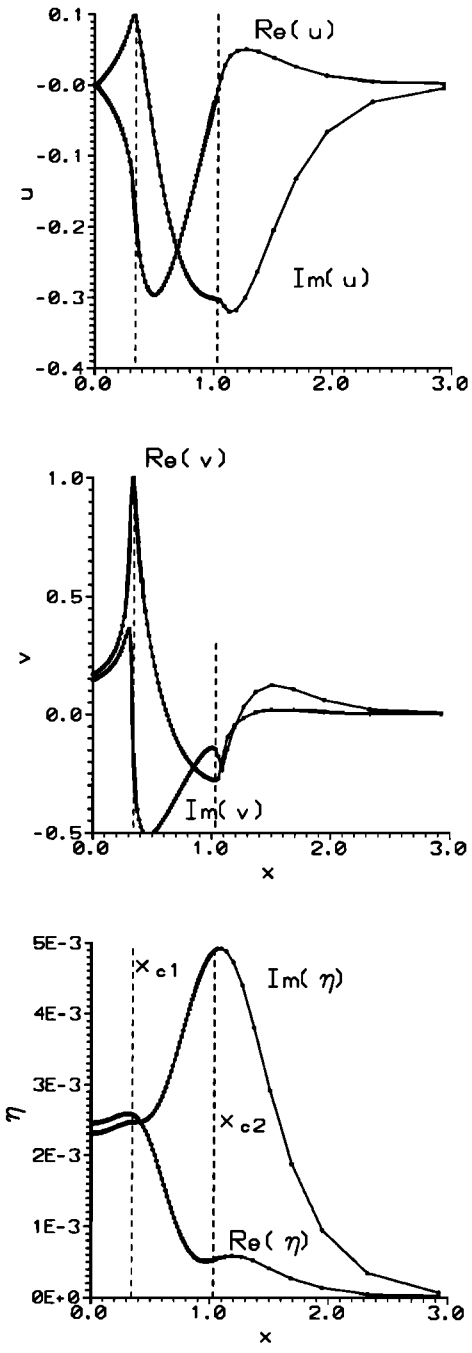


**Figure 14.** Eigensolutions of (3) for inviscid flow on a plane sloping beach with $F = 0.14$ and $k = 2.4$ near the transition. The calculation was made with $N = 120$. Note how strong velocity gradients arise near the critical points $x_{c1}$ and $x_{c2}$. On the other hand, the sea surface elevation appear to be quite smooth.

is a phase shift. The local phase relationships between wave variables are often used in field observation. Figure 16 shows the relative phase between cross-shore and longshore velocities and between cross-shore velocity and sea surface elevation for both our numerical model (plane sloping beach, $F = 0.14$) and the BH model. Interestingly, despite the numerous differences between the two models, the structures of the relative phases are very similar. Figure 17 displays the streamlines of vorticity waves (only the velocity

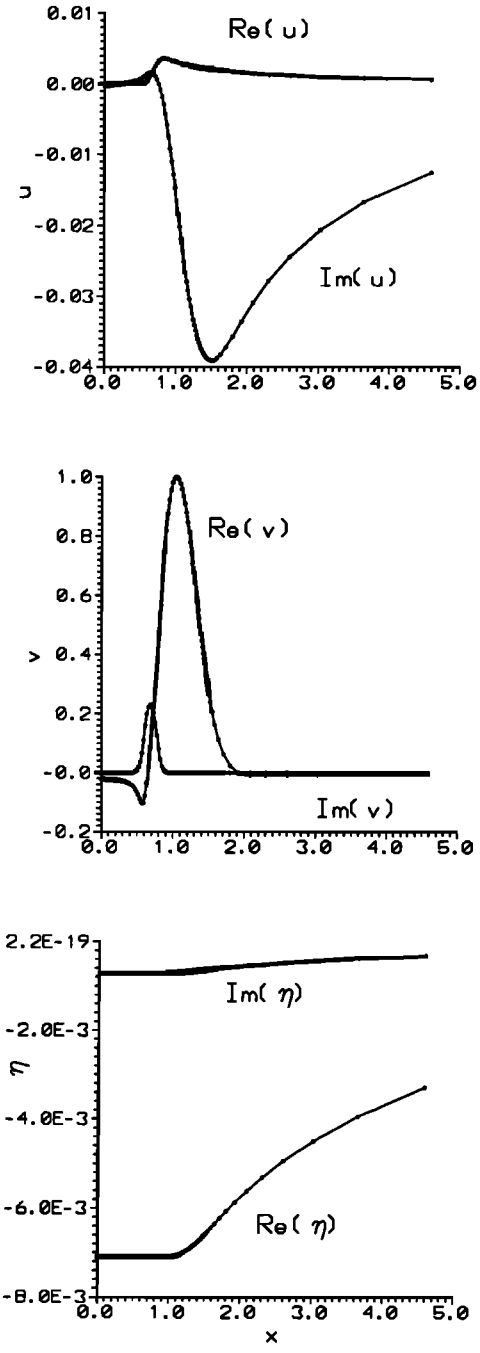


**Figure 15.** Eigensolutions of (3) for inviscid flow on a plane sloping beach with $F = 0.14$ and $k = 0.1$. For such low wavenumbers, the solution is almost real (real longshore velocity and sea surface elevation; purely imaginary cross-shore velocity).

field of the perturbation, without mean flow), showing a structure similar to that yielded by the BH model. Alongshore we find a vortex each half wavelength, with their rotation directions alternating. Cross-shore there can be one or three vortices skewing towards the longshore downstream direction. The streaming of the entire flow pattern (mean current plus perturbation) can be seen in Figure 18, where the perturbation has been scaled so that its peak magnitude equals the peak longshore current. All of these flow patterns are progressing longshore in the mean flow direction.

## 7. Discussion and Conclusions

As expected because of the similar structure of the potential vorticity profile, in broad outline our numerical simulation for realistic conditions lends support to the simplified geometry model given by BH or *Dodd and Thornton* [1990]. A similar longshore-progressing wave pattern consisting of a series of vortices is found, so adding the basic current to the flow of the perturbation results in a meandering on the perturbed flow. Typically, the longshore component of the wave field velocity is larger than the cross-shore component. The oscillations of the sea surface due to the wave are small;

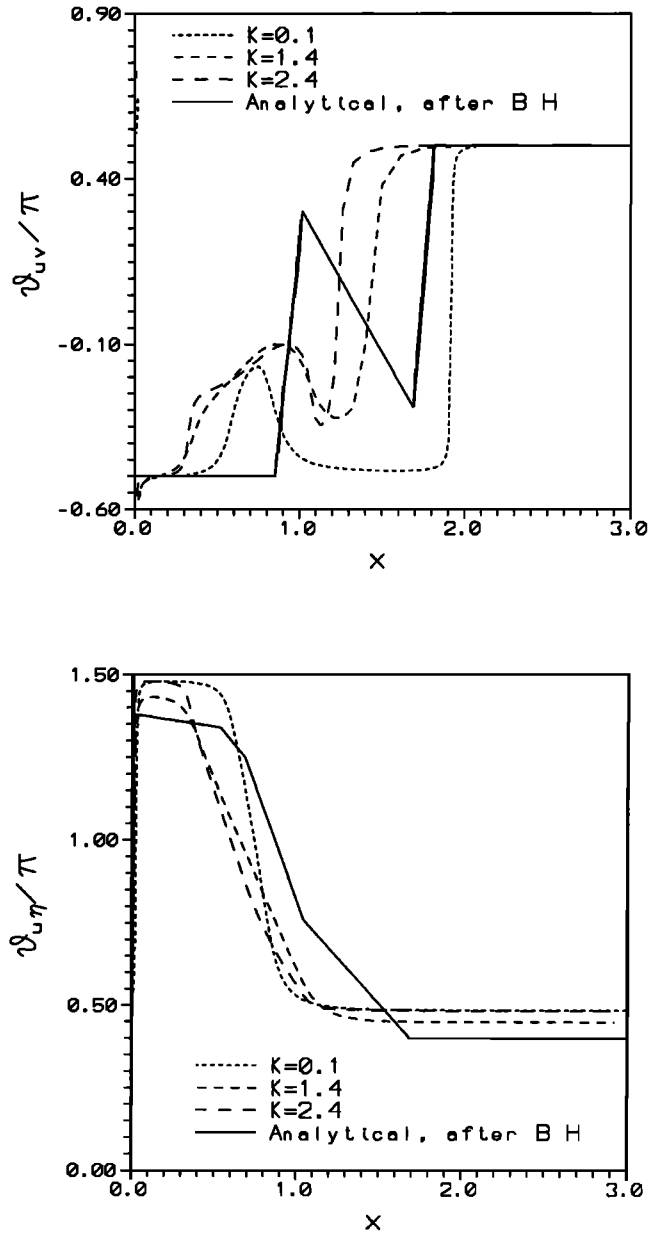


**Figure 16.** Relative phase (*a*) between longshore and cross-shore velocities and (*b*) between cross-shore velocity and sea surface elevation for inviscid flow, plane sloping beach, and $F = 0.14$ compared with results by *Bowen and Holman* [1989] (BH). We see a similar cross-shore structure. In all cases the relative phase tends to $-\pi/2$ near the coastline and to $\pi/2$ far offshore.

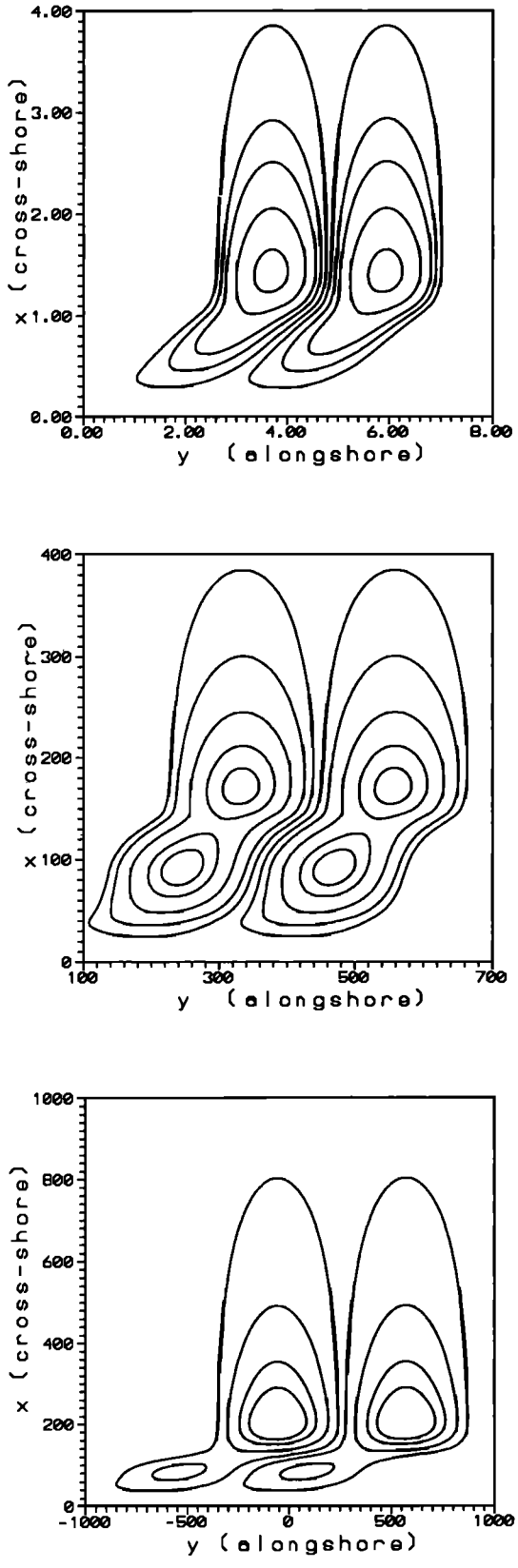


**Figure 17.** Streamlines of the vorticity wave for the fastest growing mode. The entire pattern is progressing longshore in the positive $y$ direction with the phase speed. (*a*) Inviscid flow, plane sloping beach, $F = 0.14$, $k = 1.4$. (*b*) Inviscid flow, barred beach, $k = 0.014$ m$^{-1}$. The distances are in meters. (*c*) Inviscid flow, barred beach, very low wavenumber $k = 0.005$ m$^{-1}$. The distances are in meters.

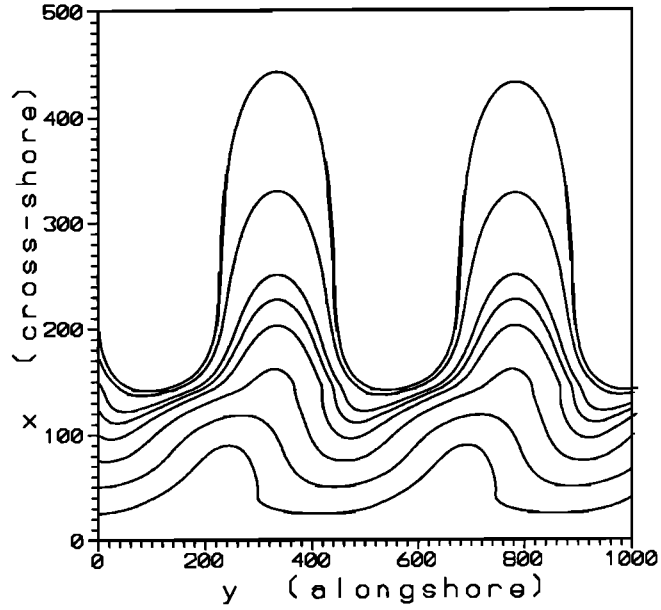


**Figure 18.** Resulting streamlines of the vorticity wave superposed on the mean flow. The arbitrary amplitude of the eigensolution has been taken so that the velocity field of the wave has the same amplitude as the mean current. Inviscid flow, barred beach, dominant mode ($k = 0.014$ m$^{-1}$). The distances are in meters.

for waves with a longshore velocity amplitude of 30 cm s$^{-1}$, we find an elevation amplitude of about 1 cm. The same cross-shore structure and even almost the same values as those found by BH are found for the phase lags between longshore and cross-shore components of the velocity and between surface elevation and cross-shore velocity. The perturbation has an offshore extension of the order of 1.5 times the width of the mean flow profile.

The validity of the usual rigid-lid assumption has been examined. We found that this approximation tends to overestimate the growth rate of the instability, so the free surface seems to produce a stabilizing effect on the flow. Frequencies are also overestimated but to a lesser extent. The differences between the free-surface and the rigid-lid solutions have been parametrized by the maximum local Froude number of the basic flow $F$ and decrease with a decreasing Froude number. For reasonably strong currents with $F = 0.6$, these differences can reach about 12% for the growth rate and 2% for the frequency. Numerical simulation for the barred beach where shear waves were first observed, with $F = 0.29$, proved that the rigid-lid assumption is indeed applicable (see Figure 12). As we can see in Figure 4, the rigid-lid assumption gives rise to appreciable errors only when the current is so strong that the frequency of some advected gravity modes (upstream edge waves) can reach the shear mode range. The explanation for this, in line with previous considerations by *Dodd and Thornton* [1990] and *Putrevu and Svendsen* [1992], is as follows. According to the beginning of section 5, $F^2$ is proportional to $V_{\max} f_s / gm$. The frequency of edge waves with a wavenumber $k$ scales as $\omega_g \sim gmk$. Shear waves scale as $\omega_s \sim f_s$ and $\omega_s / k \sim V_{\max}$. So, we have $\omega_s / \omega_g \sim F$. Therefore $F \ll 1$ corresponds to the observed situation in which gravity waves have a shorter

period than shear waves, and then the rigid-lid assumption gives rise to a good approximation. On the other hand, when $F \ll 1$ does not hold, the two time scales may be similar, with the result that both classes of motion may interact and the rigid-lid assumption may no longer be applicable.

The maximum backshear and the current width clearly provide suitable time and length scales. So, the fastest growing wavelength $\lambda_M$ is between 1.7 and 2.7 times this width, and the maximum growth rate $\omega_i$ is found to be between 0.06 and 0.15 times the maximum backshear. These results have the same order of magnitude as the previous analytical results of BH (for example, they give $\omega_i = 0.088 f_s$ for $\delta = 0.39$). Inviscid numerical simulation leads to a larger wavenumber span of the instability than the analytical models without a minimum positive unstable wavenumber (in agreement with *Putrevu and Svendsen* [1992].) Thus for inviscid flow the existence of a minimum unstable wavenumber could be a consequence of a nonsmooth current profile.

As expected, the effect of dissipation is important, resulting in a decrease in the span of unstable wavenumbers and a decrease in growth rates. There is also a small decrease in frequencies. For bottom friction or eddy viscosity giving rise to similar damping, the decrease in frequencies arising from eddy viscosity is greater than that produced by bottom friction. It is found that reasonable values of eddy viscosity or the bottom friction coefficient can entirely remove the instability in plane as well as barred beaches. For example, by using field data from Duck Beach (case D in section 5), we found that stability needs an eddy viscosity larger than $\varepsilon \sim 2.4\ \mathrm{m^2\ s^{-1}}$. Thinking of Leadbetter Beach, Santa Barbara [*Dodd et al.*, 1992], we could choose a peak velocity of $V_{\max} \sim 0.5\ \mathrm{m\ s^{-1}}$ located at $l_0 \sim 23$ m offshore, leading to $f_s = 0.024\ \mathrm{s^{-1}}$. Then according to (15), we would have a significantly smaller critical eddy viscosity, $\varepsilon \sim 0.27\ \mathrm{m^2\ s^{-1}}$. So, regarding wave-generated turbulence and assuming a similar eddy viscosity in both beaches, the flow and bathymetry at Santa Barbara would be less conducive to shear instability than those from Duck, which seems to be in agreement with experimental observations [*Dodd et al.*, 1992]. Anyway, these results indicate that a much more realistic modeling of eddy viscosity and bottom friction than the rough approach used is a must for future research.

Although the scaling and properties of the instability curves quoted above are quite generic, the details of these curves depend largely on the details of the current and depth profiles. For a plane sloping beach the instability curves are very smooth, with a monotone increase below $k_M$ and a monotone decrease above $k_M$. Instead, for a flat-bottom beach, secondary maxima are found and a mode swap similar to that found by *Putrevu and Svendsen* [1992] seems to exist. Nevertheless, the absence of any jump in the dispersion curves suggests that there are not two crossing modes but just two maxima and one minimum belonging to one mode. In fact we found (reliably) only one unstable mode in all the cases. This is in contrast with results obtained by *Dodd et al.* [1992] and *Putrevu and Svendsen* [1992], who found more than one unstable mode in some cases. This behavior might be due to the potential vorticity profiles with more than one finite extrema that they considered. Our profile for a plane sloping beach has only one finite minimum, whereas for a flat-bottom beach we also have a finite maximum at the coastline. Anyway, because of spectral pollution, one has to handle the numerical spectrum carefully, as not all the computed modes correspond to physical solutions. In the case of a barred beach, we do not find secondary maxima, but a clear inflexion appears for some wavenumbers, $k < k_M$. Moreover, considering simplified topographic profiles such as flat bottom, plane slope, etc., instead of the real barred one may give rise to variations of 50% in the growth rate and 20% in the dominant wavelength. Such results are in rough qualitative agreement with the much more extensive analysis of the influence of topography given by Putrevu and Svendsen. In general, they found a maximum instability for barred beaches, but sometimes this behavior could be reversed. In fact, in their Figure 6, some barred bathymetries have smaller growth rates than plane slopes. Anyway, we can conclude that there is a greater influence of bathymetry for barred profiles than for monotone ones. Our results are also in agreement with the suggestions by Putrevu and Svendsen that this influence comes almost exclusively from the bathymetry at the sea face of the current profile (at the backshear) and that neither the overall beach steepness nor the depth profile far from the backshear has a great influence. The kinks and humps in the instability curves appearing for a flat-bottom beach might seem to be caused by the artifact of a vertical wall at the shore. However, by handling exponential beach profiles with several slopes at the coastline (case C in section 5), we found a continuous transition from instability curves with a secondary maximum to the smooth ones for a plane sloping beach. The details of the current profile may also significantly influence instability curves. This can be seen in Figures 7 and 8, where, for example, going from $n = 3$ to $n = 2$ inverts the absolute and secondary maxima. This is in agreement with results obtained by *Dodd et al.* [1992] (Figure 6), where for very similar current profiles they get a quite different pattern. We conclude that these kind of kinks and humps in the instability curves are probably due to the flatness of the bottom near the peak and at the backshear of the mean flow profile but also have a great sensitivity to the actual flow profile in this area.

Quite linear dispersion relations similar to that obtained by BH and that observed by *Oltman-Shay et al.* [1989] are found. However, as in the numerical simulations mentioned above, the dispersion curves have a (0, 0) intercept, in contrast to the experimental ones. As was pointed out by *Dodd et al.* [1992], this difference appears to be an artifact of the experimental data analysis (finite frequency bin width). Concerning the phase speed of the waves, we found a phase velocity of about 0.5 to 0.7 times the mean longshore current peak, which was larger than values determined by BH, giving rise to $0.3 V_{\max}$ for a piecewise linear shear flow similar to our smooth profile. According to the phase speed larger than that in BH, we also obtain larger frequencies for the fastest growing mode $f$, that is, about 0.08 to 0.1 times $f_s$. The possible phase speeds of neutral shear waves were analytically shown to be given by the velocity of the mean flow at the cross-shore locations where the potential vorticity has some extremum. Although this statement is valid only for neutral waves, for the cases under study we found that the phase speed of growing modes is not far from this value, with the result that this velocity gives rise to an estimate of the phase velocity of growing shear waves. The estimated velocity exceeds the phase speed of the fastest growing mode by 13% for a plane sloping beach and by 30%

for the barred beach considered. Dissipation does not have a great influence on the frequencies and the phase speed. We found a small decrease of less than 9% in the phase speeds of growing modes.

Field data reported by *Oltman-Shay et al.* [1989, Table 1] show phase speeds of between 0.71 and 0.80 times the mean current at the trough of the longshore bar. If the actual current profile were like that shown in Figure 1, we might expect the velocity at this location to be about $0.7V_{max}$. Hence we can consider experimental data to exhibit a phase speed of 0.51 to 0.58 times the mean current peak, whereas our numerical simulation for the true beach topography gives $0.55V_{max}$. Very similar results were obtained by *Putrevu and Svendsen* [1992] in their numerical simulation (0.5 to 0.6 times $V_{max}$). Nevertheless, a more accurate current profile modeling [*Dodd et al.*, 1992] gives rise to a higher ratio between the velocity at the trough of the bar and the current peak. So, higher $c_r/V_{max}$ ratios (between 0.6 and 0.9) are obtained. Numerical simulation by these authors gave rise to ratios of 0.6 to 0.8. In summary, according to the current and beach profiles chosen for the numerical simulation, there is a great deal of variability of $c_r/V_{max}$, between 0.5 and 0.8. On the other hand, field observation does not give accurate ratios because of the large error bars in the current profile and in $V_{max}$. So, giving an accurate prediction of $c_r/V_{max}$ is very difficult.

Finally, the classical energy analysis of the *Drazin and Reid* [1981, p. 142] semicircle theorem has been extended to allow for a free upper surface. By this method we could not obtain a semicircle bound on $c$ but only the Rayleigh condition $V_{min} < c_r < V_{max}$ when $c_i \neq 0$. Nevertheless, by numerical simulation we could not find any counterexample against the semicircle bound either.

**Acknowledgments.** We are very grateful to N. Dodd for the helpful discussions we had before and during his visit to our university and especially for suggesting that we look more in depth at the validity of the rigid-lid assumption. We would like to thank J. Sanchez for his advice on some numerical aspects of the present work. Thanks are also due to the anonymous referees for their useful advice. This work has been funded by the UPC under grant PR9126 and the DGYCIT under grant PB91-0594.

## References

Bowen, A. J., and R. A. Holman, Shear instabilities of the mean longshore current, 1, Theory, *J. Geophys. Res.*, *94*(C12), 18,023–18,030, 1989.

Boyd, J. B., Orthogonal rational functions on a semi-infinite interval, *J. Comput. Phys.*, *70*, 63–88, 1987.

Boyd, J. B., Chebyshev and Fourier spectral methods, *Lecture Notes in Engineering*, *49*, pp. 1–70, Springer-Verlag, New York, 1989.

Canuto, C., M. Y. Hussaini, A. Quarteroni, and T. A. Zang, *Spectral Methods in Fluid Dynamics*, Springer-Verlag, New York, 1988.

Dodd, N., and E. B. Thornton, Growth and energetics of shear waves in the nearshore, *J. Geophys. Res.*, *95*(C9), 16,075–16,083, 1990.

Dodd, N., J. Oltman-Shay, and E. B. Thornton, Shear instabilities in the longshore current: A comparison of observation and theory, *J. Phys. Oceanogr.*, *22*(1), 62–82, 1992.

Drazin, P. G., and W. H. Reid, *Hydrodynamic Stability*, Cambridge University Press, New York, 1981.

Falqués, A., and V. Iranzo, Edge waves on a longshore shear flow, *Phys. Fluids A*, *4*(10), 2169–2190, 1992.

Howd, P. A., A. J. Bowen, R. A. Holman, and J. Oltman-Shay, Infragravity waves, long-shore currents and sand bar formation, in *Coastal Sediments 91*, pp. 72–84, American Society of Civil Engineers, New York, 1991*a*.

Howd, P. A., J. Oltman-Shay, and R. A. Holman, Wave variance partitioning in the trough of a barred beach, *J. Geophys. Res.*, *96*(C7), 12,781–12,795, 1991*b*.

Howd, P. A., A. J. Bowen, and R. A. Holman, Edge waves in the presence of strong longshore currents, *J. Geophys. Res.*, *97*(C7), 11,357–11,371, 1992.

Iranzo, V., and A. Falqués, Some spectral approximations for differential equations in unbounded domains, *Comput. Methods Appl. Mech. Eng.*, *98*, 105–126, 1992.

Llobet, X., K. Appert, A. Bondeson, and J. Vaclavik, On spectral pollution, *Comput. Phys. Commun.*, *59*, 199–216, 1990.

Oltman-Shay, J., P. A. Howd, and W. A. Birkemeier, Shear instabilities of the mean longshore current, 2, Field observations, *J. Geophys. Res.*, *94*(C12), 18,031–18,042, 1989.

Putrevu, U., and I. A. Svendsen, Shear instability of longshore currents: A numerical study, *J. Geophys. Res.*, *97*(C5), 7283–7303, 1992.

van Rijn, L. C., Mathematical modelling of morphological processes in the case of suspended sediment transport, Ph.D. thesis, *Commun. 382*, Delft Hydraul., Delft, Netherlands, 1987.

A. Falqués and V. Iranzo, Departament de Física Aplicada, Universitat Politècnica de Catalunya, Jordi Girona Salgaso, s/n, 08034 Barcelona, Spain.

(Received September 30, 1992; revised March 25, 1993; accepted June 22, 1993.)